AFRL-RQ-WP-TP-2014-0242

VOLTAGE AND PRESSURE SCALING OF STREAMER DYNAMICS IN A HELIUM PLASMA JET WITH N_2 CO-FLOW (POSTPRINT)

Robert J. Leiweke

UES, Inc.

Biswa N. Ganguly and James D. Scofield

Electrical Systems Branch
Power and Control Division

AUGUST 2014

AIR FORCE RESEARCH LABORATORY
AEROSPACE SYSTEMS DIRECTORATE
WRIGHT-PATTERSON AIR FORCE BASE, OH 45433-7541
AIR FORCE MATERIEL COMMAND
UNITED STATES AIR FORCE

NOTICE AND SIGNATURE PAGE

This report was cleared for public release by the USAF 88th Air Base Wing (88 ABW) Public Affairs Office (PAO) and is available to the general public, including foreign nationals.

Copies may be obtained from the Defense Technical Information Center (DTIC) (http://www.dtic.mil).

AFRL-RQ-WP-TP-2014-0242 HAS BEEN REVIEWED AND IS APPROVED FOR PUBLICATION IN ACCORDANCE WITH ASSIGNED DISTRIBUTION STATEMENT.

*//Signature//
JAMES D. SCOFIELD
Program Engineer
Electrical Systems Branch
Power and Control Division

//Signature//
GREGORY L. FRONISTA, Chief
Electrical Systems Branch
Power and Control Division
Aerospace Systems Directorate

REPORT DOCUMENTATION PAGE

Form Approved
OMB No. 0704-0188

1. REPORT DATE *(DD-MM-YY)*	2. REPORT TYPE	3. DATES COVERED *(From - To)*
August 2014	Journal Article Postprint	01 June 2012 – 31 May 2014

4. TITLE AND SUBTITLE
VOLTAGE AND PRESSURE SCALING OF STREAMER DYNAMICS IN A HELIUM PLASMA JET WITH N_2 CO-FLOW (POSTPRINT)

5a. CONTRACT NUMBER
In-house

5b. GRANT NUMBER

5c. PROGRAM ELEMENT NUMBER
61102F

6. AUTHOR(S)
Robert J. Leiweke (UES, Inc.)
Biswa N. Ganguly and James D. Scofield (AFRL/RQQE)

5d. PROJECT NUMBER
3001

5e. TASK NUMBER
N/A

5f. WORK UNIT NUMBER
Q12A

7. PERFORMING ORGANIZATION NAME(S) AND ADDRESS(ES)
UES, Inc.
4401 Dayton-Xenia Road
Dayton, OH 45432

Electrical Systems Branch (AFRL/RQQE)
Power and Control Division
Air Force Research Laboratory, Aerospace Systems Directorate
Wright-Patterson Air Force Base, OH 45433-7541
Air Force Materiel Command, United States Air Force

8. PERFORMING ORGANIZATION REPORT NUMBER
AFRL-RQ-WP-TP-2014-0242

9. SPONSORING/MONITORING AGENCY NAME(S) AND ADDRESS(ES)
Air Force Research Laboratory
Aerospace Systems Directorate
Wright-Patterson Air Force Base, OH 45433-7541
Air Force Materiel Command
United States Air Force

10. SPONSORING/MONITORING AGENCY ACRONYM(S)
AFRL/RQQE

11. SPONSORING/MONITORING AGENCY REPORT NUMBER(S)
AFRL-RQ-WP-TP-2014-0242

12. DISTRIBUTION/AVAILABILITY STATEMENT
Approved for public release; distribution unlimited.

13. SUPPLEMENTARY NOTES
PA Case Number: 88ABW-2014-3646; Clearance Date: 08 Aug 2014.

Report published in *Physics of Plasmas*, Vol. 21, 2014.

14. ABSTRACT

Positive polarity applied voltage and gas pressure dependent scaling of cathode directed streamer propagation properties in helium gas flow guided capillary dielectric barrier discharge have been quantified from streamer velocity, streamer current, and streamer optical diameter measurements. All measurements of the non-stochastic streamer properties have been performed in a variable gas pressure glass cell with N_2 co-flow and under self-consistent Poisson electric field dominated conditions to permit data comparison with 2-D streamer dynamics models in air/nitrogen. The streamer optical diameter was found to be nearly independent of both gas pressures, from 170 Torr up to 760 Torr, and also for applied voltages from 6 to 11 kV at 520 Torr. The streamer velocity was found to increase quadratically with increased applied voltage. These observed differences in the 2-D scaling properties of ionization wave sustained cathode directed streamer propagation in helium flow channel with N_2 annular co-flow compared to the streamer propagation in air or nitrogen have been shown to be caused by the remnant ionization distribution due to large differences in the dissociative recombination rates of He_2^+ versus N_4^+ ions, for this 5 kHz repetition rate applied voltage pulse generated streamers.

15. SUBJECT TERMS

16. SECURITY CLASSIFICATION OF:			17. LIMITATION OF ABSTRACT:	18. NUMBER OF PAGES	19a. NAME OF RESPONSIBLE PERSON (Monitor)
a. REPORT	b. ABSTRACT	c. THIS PAGE			James D. Scofield
Unclassified	Unclassified	Unclassified	SAR	18	19b. TELEPHONE NUMBER *(Include Area Code)* N/A

Voltage and pressure scaling of streamer dynamics in a helium plasma jet with N_2 co-flow

Robert J. Leiweke,[1] Biswa N. Ganguly,[2] and James D. Scofield[2]
[1]*UES, Inc., 4401 Dayton-Xenia Road, Dayton, Ohio 45432, USA*
[2]*Air Force Research Laboratory, Wright-Patterson Air Force Base, Ohio 45433-7919, USA*

(Received 12 May 2014; accepted 21 July 2014; published online 14 August 2014)

Positive polarity applied voltage and gas pressure dependent scaling of cathode directed streamer propagation properties in helium gas flow guided capillary dielectric barrier discharge have been quantified from streamer velocity, streamer current, and streamer optical diameter measurements. All measurements of the non-stochastic streamer properties have been performed in a variable gas pressure glass cell with N_2 co-flow and under self-consistent Poisson electric field dominated conditions to permit data comparison with 2-D streamer dynamics models in air/nitrogen. The streamer optical diameter was found to be nearly independent of both gas pressures, from 170 Torr up to 760 Torr, and also for applied voltages from 6 to 11 kV at 520 Torr. The streamer velocity was found to increase quadratically with increased applied voltage. These observed differences in the 2-D scaling properties of ionization wave sustained cathode directed streamer propagation in helium flow channel with N_2 annular co-flow compared to the streamer propagation in air or nitrogen have been shown to be caused by the remnant ionization distribution due to large differences in the dissociative recombination rates of He_2^+ versus N_4^+ ions, for this 5 kHz repetition rate applied voltage pulse generated streamers. © *2014 AIP Publishing LLC*.
[http://dx.doi.org/10.1063/1.4892968]

I. INTRODUCTION

Highly non-equilibrium atmospheric pressure plasma jets have recently been investigated for producing active plasmas under ambient conditions. One specific type of such plasma jet that allows the formation of a non-stochastic active discharge extending beyond the anodic electrode uses a capillary dielectric tube with helium gas flow under ambient conditions. Several experimental[1–8] and modeling[9–14] results of such helium plasma jets have been published which show that this type of discharge behaves like a cathode directed streamer propagation. This plasma jet uses a dielectric barrier configuration with annular anode configured as a co-axial electrode with the helium gas flow, in contrast to a point-to-plane electrode configuration normally used for streamer propagation in air or in nitrogen. The gas dielectric breakdown and self-sustained streamer propagation are possible to achieve in the helium gas channel at a much lower reduced electric field compared to the co-flowing and/or surrounding air. These differences in electrical characteristics[15] of streamer propagation in helium versus air[16,17] are responsible for the observed differences in the propagation of ionization wave sustained streamer propagation in helium flow channel in ambient air compared to the streamer propagation in air or nitrogen.[17–26] Although many experimental results and model calculations have been published for streamer propagation in the helium flow channel in ambient air, a systematic study of applied voltage and/or pressure dependent two-dimensional or three dimensional scaling properties of the streamer launched by this capillary dielectric barrier discharge (CDBD) with annular anodic electrode, compared to point-to-plane streamer propagation in air, have not yet been published. In this work, we report measurements of applied voltage and gas pressure dependent scaling properties of streamer current, streamer speed, and streamer radiative channel diameter[17] with co-flowing nitrogen.

In order to control the purity of the co-flowing gas and avoid the effects of ambient room air current, the capillary dielectric tube with annular anode was placed inside a 3 cm diameter glass enclosure where the gas pressure was controlled by a downstream pump and flow controller. One of the advantages of controlling the co-flow gas is that the plasma jet propagation can be maintained over a relatively long length as the total gas pressure is varied from 760 Torr down to 170 Torr. This glass enclosed cell experimental condition is very well suited for the systematic study of the streamer scaling properties in lower dielectric breakdown strength gases surrounded by much higher dielectric breakdown strength gases. The ring anode electrode used in this CDBD configuration produces a Laplacian electric field in addition to the self-consistent Poisson electric field of the streamer.[10] In order to study the voltage and gas pressure dependent scaling properties of streamer propagation under the influence of low external applied electric field and streamer dynamics properties dominated by the self-consistent Poisson electric field, it is required to measure streamer scaling properties at locations far away from the ring anode. This glass cell enclosed plasma jet configuration permits us to measure streamer velocity, streamer radiative channel diameter, and streamer current scaling with the variation of both applied voltage and gas pressure under the conditions of low applied external electric field. We have used spatio-temporally resolved imaging of spectrally resolved plasma

emission from the helium 3^3D-2^3P transition to measure streamer velocity and streamer radiative channel diameter. We have also measured spatially (1 mm at the focal volume) and temporally ($\pm$ 2 ns) resolved optical emission from He 3^3S- 2^3P at 706.5 nm, 391 nm N_2^+ ($B^2\Sigma_u^+ \rightarrow X^2\Sigma_g^+$), and 337.1 nm emission from N_2 $C^3\Pi_u$-$B^3\Pi_g$ using optical fiber coupled photomultipliers. Of these, the 587.6 and 706.5 nm emission lines from atomic helium provided accurate signatures for direct electron impact ionization of helium at the streamer head. If the direct electron impact ionization of helium and nitrogen gases are occurring at the streamer head,[12] then dual optical fiber channel coupled photomultipliers should detect those signatures from our simultaneous optical emission intensity measurements.

Experimental details and experimental results of two-dimensional scaling behavior of the streamers in lower dielectric breakdown strength helium gas surrounded by much higher dielectric breakdown strength nitrogen gas are discussed below. A zero dimensional plasma chemical kinetics model has been used to show the influence of remnant ionization on the streamer propagation properties of the non-stochastic helium plasma jet for 5 kHz repetition rate pulsed excitation.

II. EXPERIMENTAL DETAILS

Figure 1 shows the helium plasma jet, powered by a single copper ring anode, mounted coaxially inside a 30 mm inner diameter cylindrical glass cell having a co-flow of nitrogen. Downstream from the plasma jet assembly, the cell gas pressure was automatically monitored and maintained at pressures ranging from 760 Torr down to 170 Torr while a mechanical vacuum pump was used to evacuate the gases. The glass capillary was 6 cm long with an inner diameter of 2 mm and an outer diameter of 3 mm. As shown in Figure 1, a 2 cm long copper ring electrode was placed 2 mm from the capillary tip. For all conditions reported in this paper, helium gas flowed through the capillary at 2 standard liters per minute (SLM) resulting in an exit flow speed of $\approx$17 m/s. The co-flowing nitrogen background gas was introduced into the cell 25 cm behind the capillary tip at a volume flow rate of 0.5 SLM. Based on the inner diameter, the Reynolds number for the helium flow at the capillary tube exit was about 190 at 520 Torr.

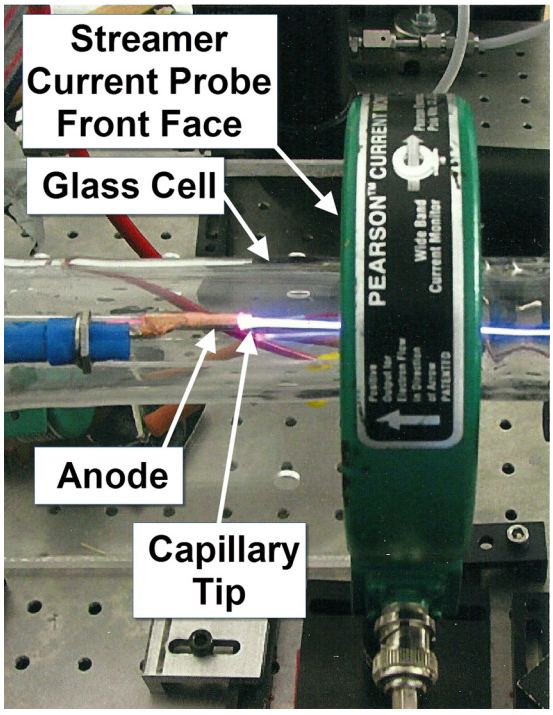

FIG. 1. Visible emission photograph of the 2 SLM helium plasma jet operating within the glass cell with a 0.5 SLM N_2 annular co-flow at 520 Torr excited by 9 kV unipolar total applied voltage pulses.

Unipolar, high voltage pulses (6–12 kV) having a 20 ns rise time were applied to the copper ring anode at a 5 kHz pulse repetition rate via an electrical feed through in the glass cell wall. For the time-averaged streamer plasma emission image at 520 Torr, shown in Figure 1, the peak total applied voltage at the anode was 9 kV measured at the high voltage switch, prior to a 300 Ω ballast resistor, using a 1000:1 high voltage probe (North Star PVM-11). The total circuit current was measured at the powered anode wire using an annular wide-bandwidth current sensor (Pearson model 4100, 1 V/A). Also shown in Figure 1, the streamer current was measured by symmetrically threading the glass cell through the 5 cm inner diameter hole of an annular wide-bandwidth current sensor (Pearson model 6585, 1 V/A). Unless otherwise noted, the front face of the streamer current sensor was located 23 mm from the capillary tip for all experimental conditions. The time-averaged broad band visible emission from the plasma jet, as shown in Figure 1, implies that the streamer discharge propagated through the 25 mm wide current probe and then at least another 2 cm further downstream under this gas flow condition. All time-dependent voltage and current measurements were acquired with a 4-channel, 500 MHz bandwidth oscilloscope (LeCroy 6050), 1000 samples averaged, and then transferred to a desktop computer for analysis.

A gated intensified charge-coupled device (ICCD) camera (Princeton Instruments PI-MAX I, 512×512 CCD pixel arrays) was used to collect spatiotemporally resolved atomic helium 3^3D-2^3P emission at 587.6 nm using a 10 nm band pass filter (Thorlabs FB590-10-1) mounted at the front of the camera lens system. The He 3^3D-2^3P transition was chosen because it has a direct electron impact excitation threshold energy of 23.1 eV, compared to 24.6 eV for ionization, and a relatively large spontaneous emission coefficient ($A_{12} \approx 7 \times 10^7\ s^{-1}$, Ref. 27), making it a sensitive marker for direct electron impact excitation at/or near the streamer head. The imaging optical axis was perpendicular to the capillary axis. The camera collection optics consisted of a BK-7 telecentric and zoom lens combination with several extender rings and a working distance of 170 mm, resulting in a 1:1 magnification of the optical collection system. The 12 mm field of view along the streamer propagation axis was between 6 mm and 18 mm from the capillary tip, and the image resolution was $\approx$150 μm, corresponding to $\sim$6 pixels. Unless otherwise noted, all images were acquired using a 5 ns ICCD gate on-time, 40 000 accumulated ICCD exposures, and a fixed intensifier gain setting.

III. RESULTS

A. 520 Torr data

We have chosen to use 520 Torr closed cell pressure for initial sets of measurements since it allowed us to measure streamer scaling properties over a wide voltage range without surface flashover in our configuration. Compared to the open plasma jet configuration at 760 Torr, it also allowed us to control the co-flowing gas compositions.

Figure 2 shows a typical example of the current and voltage traces acquired for the plasma jet operating at a peak total applied voltage of 9 kV using N_2 as the co-flowing background gas. Note that the timescale in Figure 2 is relative to the peak total circuit displacement current. The total circuit current and applied voltage were synchronized to an accuracy of ±2 ns by temporally shifting and rescaling the time integrated displacement current and matching the amplitude to that of the applied voltage temporal signal. The streamer current was obtained by first acquiring a background trace from the streamer current probe with the helium flow turned off, but with the applied voltage on (discharge off condition). This background trace was stored in the oscilloscope memory and then subtracted from the real time streamer probe signal. With the resumption of helium flow, the discharge was turned back on and steady state conditions were established. Ten real time streamer current samples were acquired and then averaged during post processing. Non-random noise fluctuations "ringing" due to circuit effects were mitigated using adjacent average time-step filtering (OriginPro 8.1 software package[28]). For each discharge condition, the signal filtering was carefully chosen to preserve both the rise time, peak, and decay time features. The signal propagation delay with respect to the total circuit current was accounted for by temporally shifting the onset time of the streamer probe background trace so that it matched the onset time of the total circuit displacement current with about ±3 ns accuracy. This delay time correction was applied to the mean streamer current trace. For the 9 kV peak applied voltage, in Figure 2, the measured peak streamer current was 20 mA, and an estimated upper bound of 60 μJ energy was deposited into the streamer.

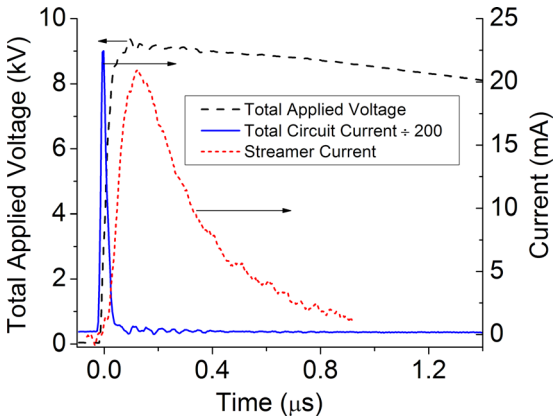

FIG. 2. Measured total applied voltage (dashed line), total circuit current, and streamer current (dotted line) for the helium plasma jet excited by 9 kV peak unipolar high voltage pulses at 5 kHz pulsed repetition rate.

Streamers generated by CDBD helium plasma jets operating in air are known to exhibit an annular morphology having an outer diameter that is initially approximately equal to the capillary tube inner diameter.[8,10,14,29] The ring-like shape is formed due to the initial Laplacian electric field that induces breakdown near the inner wall of the dielectric tube.[8,10,14,29] As the streamer propagates away from the capillary tip, confined within the helium gas jet, the annular radius tends to decrease towards the centerline axis and may eventually converge on axis.[8,10,14,29] From the two dimensional ICCD emission images, radial intensity slice plots were obtained using Image J imaging analysis software[30] for applied voltages from 6–10 kV. Both the two dimensional emission intensity images and radial slice plots showed that the streamer head exhibited a symmetric annular structure that converged on-axis approximately 8 mm from the capillary tip. Axial slice plots obtained from late time emission intensity images (not shown) for which the streamer had moved well past the field of view showed on-axis He 587.6 nm emission attributed to the Laplacian electric field extending beyond 8 mm up to approximately 12 mm (recall that the total applied voltage fall time was ~8 μs). Taken together, the information obtained from these ICCD images indicates that the streamer head radial emission profile exhibited a morphological transition from ring-like near the capillary tip to Gaussian-like at 16 mm from the capillary tip. At this 16 mm location, the influence of the Laplacian electric field on the streamer head was negligible (discussed below in Sec. III B) and behaves more like a cathode directed positive streamer with low applied electric field (in Sec. III B, we illustrate this transition in Figure 8 which shows ICCD radial emission intensity slice plots at 6 mm and 16 mm axial positions obtained at 365 Torr and 6 kV applied voltage). For this reason, we have chosen the 16 mm axial location for comparing streamer scaling properties with model calculations in helium and air[10–12,17–20] and also measurements[17,22–26] in air and nitrogen, where streamer scaling properties are determined by space-charge induced Poisson electric field at the streamer head.

Figure 3 shows the scaling of peak streamer current with peak total applied voltage taken at two different locations of the current probe at 520 Torr. The square symbols represent the data with the current sensor front face located 23 mm from the capillary tip. The circles represent the peak current scaling for conditions with the front face of the Pearson probe located 33 mm from the capillary tip. Also shown in Figure 3 are best-fit polynomial lines through the data points which indicate a quadratic scaling of peak current increase with increasing voltage. We define the meaning of the "best fit" as that polynomial expression which, statistically, best describes the data set using the lowest degree possible with a 95% confidence level constraint. The assessment of the minimal degree required was performed by sequentially testing four sets of polynomials ranging from fourth order down to first order using Analysis of Variance (ANOVA) error-weighted polynomial regression.[28,31] The quadratic dependence of streamer current with applied voltage shown in Figure 3 is in agreement with 1-D analysis and 2-D modeling

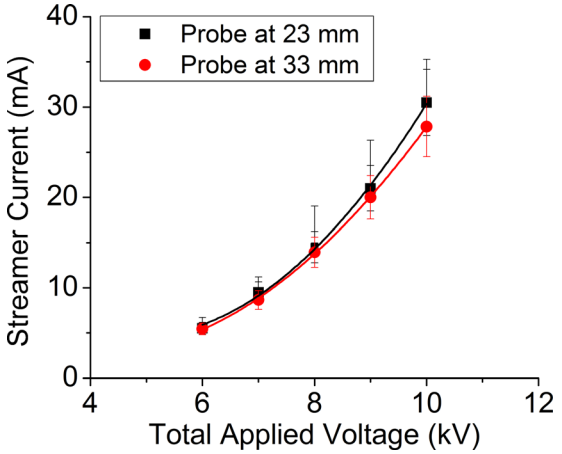

FIG. 3. Measured peak streamer current as a function of total applied voltage at 520 Torr with the probe front face located 23 mm (squares) and 33 mm (circles) from the capillary tip. The solid lines are quadratic best fits (see text) to the data points.

for positive streamer propagation in homogeneous air.[18] As the current probe was moved from 23 mm to 33 mm from the capillary tip, the streamer current remains nearly unchanged. This suggests that diffusional mixing of the annular co-flow gas into the helium core flow can be neglected at positions approximately up to 33 mm from the capillary tip.

Figure 4 shows the scaling of streamer velocity increase with total peak applied voltage when the maximum streamer head emission intensity was located between 15 and 16 mm from the capillary tip. These measurements were performed simultaneously with the peak streamer current measurements shown in Figure 3. The streamer speeds for each discharge condition were derived from sequentially time delayed gated ICCD camera images of the He 587.6 nm emission at the streamer head within the imaging field of view between 6 mm and 18 mm from the capillary tip. Using a 5 ns gate width, the intensifier gate delay was adjusted so that at least three (depending upon the streamer speed) background subtracted images having a temporal separation no more than 5 ns apart were acquired. For this 2-D axisymmetric geometry, the streamer head propagation direction is collinear with the electric field, so the measured streamer speed should be same as the streamer head velocity. From these images, 10-pixel radial binned average intensity slice plots cutting across the entire image along the propagation axis and through the streamer head axial centerline were obtained using ImageJ. From these emission intensity slice plots, the average streamer velocities were estimated by dividing the change between the 90% peak height axial positions of temporally successive slice-plot pairs by the change in their respective gate delay times. It should be noted that the estimated streamer velocities at each applied voltage were nearly constant (within the 10% uncertainty of the measurements) between 14 mm and 17 mm from the capillary tip. As shown in Figure 4, by the minimum polynomial fit of the data, the streamer velocity increase scaled *quadratically with increased applied voltage*. Both measurements[26] and modeling[18] in air have predicted a linear relationship between positive streamer velocity and applied voltage for streamer propagation in homogeneous air. It is not known if our measurement results, which indicate quadratic streamer velocity scaling with increased applied voltage is due to a departure from the velocity-diameter scaling (see next paragraph) observed for streamer propagation in air[20,21,26] or due to "streamer coupling for glow like discharge"[13] in the helium gas channel with high degree of remnant ionization in the 5 kHz pulse repetition rate condition (see Sec. IV).

Figure 5 shows a plot of the streamer head radiative channel "optical" diameter (FWHM) located 16 mm from the capillary tip as a function of total applied voltage obtained from ICCD image emission intensity radial slice plots (radial profiles obtained at 6 kV and 8 kV at 520 Torr are shown in Figures 9(a) and 9(b)). The set of optical diameter measurement values are also listed in Table I. We note that these measurements were performed simultaneously with the streamer current measurements shown in Figure 3 with the probe front face located 23 mm from the capillary tip and were also obtained from the same images used to estimate the streamer speeds shown in Figure 4. Both Figure 5 and Table I show that the streamer head optical diameters are essentially independent of the applied voltage. Note that the optical diameters change 14% from 0.63 mm at 6 kV to

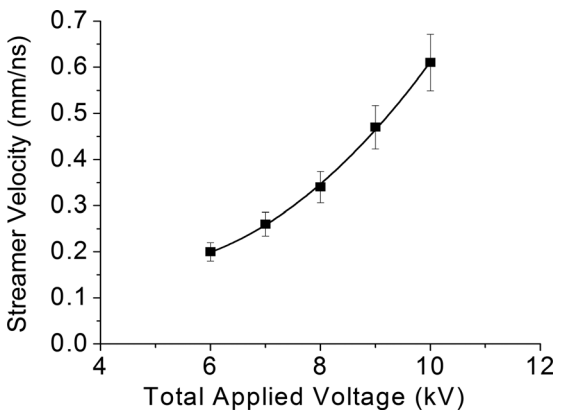

FIG. 4. Streamer velocity as a function of total applied voltage at 520 Torr. The streamer head was located 16 mm from the capillary tip. The solid line is a quadratic best fit to the data points (see text).

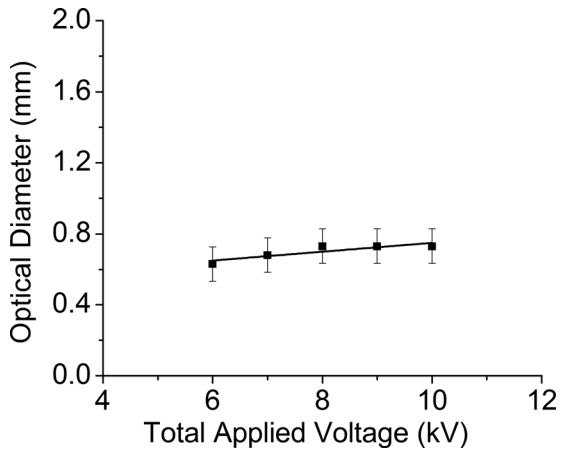

FIG. 5. Streamer optical diameters (FWHM) as a function of total applied voltage at 520 Torr. The streamer head was located 16 mm from the capillary tip. The solid line is a linear best fit to the data points (see text).

TABLE I. Optical diameters at the streamer head measured 16 mm from the capillary tip using ICCD imaging of the He 587.6 nm emission intensity. Also shown are electron number density estimates as a function of applied voltage at 520 Torr. The uncertainty of the diameter measurements are ±13% while that of the number density estimates are ±20%.

Applied voltage (kV)	D (mm)	n_e ($\times 10^{11}$ cm^{-3})
6	0.63	5.5
7	0.68	6.3
8	0.73	6.4
9	0.73	6.7
10	0.73	7.5

0.73 mm at 10 kV while the corresponding streamer velocities shown in Figure 4 exhibit a 70% increase from 0.20 mm/ns to 0.61 mm/ns between 6 and 10 kV. The lower values of optical diameter at 6 kV and 7 kV applied voltages (see Table I) are attributed to the lower ICCD imaging S/N ratio. As mentioned above, the radial ICCD emission intensity profiles were Gaussian-like at the 16 mm position (for example, see Sec. III B Figures 8, 9(a), and 9(b)). The diameters near the baseline using a 2 ns ICCD gate were approximately 0.2 mm smaller than those acquired using a 5 ns gate time, a difference that is near the imaging system resolution and can be attributed to a lower S/N ratio rather than the effect of "blurring" due to axial translation during the exposure time. The FWHM optical diameters were only sensitive to the 2 ns ICCD gate time at 6 kV and 7 kV and were again within the imaging system resolution. We chose the FWHM optical diameter to be the metric for the streamer head diameter because of the better S/N ratio and as a standard for comparison to other streamer data in the literature.[17,24,26]

Figure 6 shows the velocity-diameter plot for the same data taken from Figures 4 and 5. Because the optical diameters are nearly constant as a function of applied voltage (see Table I and Figure 5), the streamer velocity is independent of optical diameter for the applied voltage range of 6–10 kV. This velocity-diameter scaling in the helium plasma jet exhibits a strong departure from measurements[24,26] and modeling results[18] of positive streamers in air. *The invariance of the optical diameter with applied voltage and streamer velocity is a consequence of both the lower dielectric breakdown strength of the helium gas channel compared to the surrounding nitrogen co-flow, which has a much higher breakdown electric field requirement*,[8,10] but, more importantly, it may be due to remnant ionization in pure helium core flow versus helium-nitrogen boundary layer for this 5 kHz repetition rate pulsed discharge.

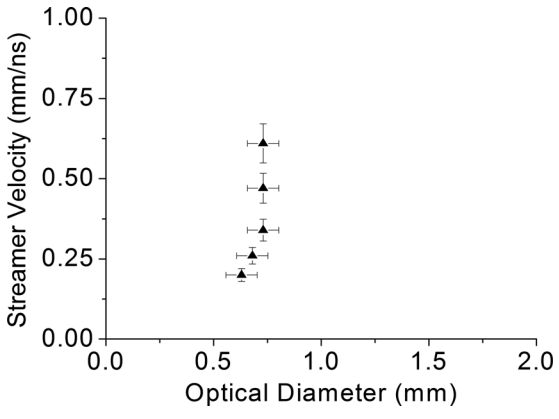

FIG. 6. Streamer velocity as a function of optical diameter at 520 Torr. The streamer head was located 16 mm from the capillary tip.

We were not able to quantify accurately the scaling of the streamer head emission axial FWHM with applied voltage from the ICCD images due to axial "blurring" of the propagating streamer head within the 5 ns ICCD camera gate time. However, we have used images taken with 5 ns and 2 ns gate times and extrapolated the axial FWHM to near 0 ns gate time for the condition when the current probe front face was located 23 mm from the capillary tip. Assuming a linear relationship between the axial FWHM and gate time, an extrapolation to 0 ns gate time resulted in an axial FWHM between 0.6 mm at 8 kV to 1.4 mm at 10 kV. Again, these characteristics of the radial versus axial electron impact excitation profiles in helium seem to be different compared to streamers in air.[18–20]

Electron number density estimates behind the streamer head for each applied voltage pulse have been made using the one dimensional current continuity approximation,

$$n_e = \frac{4I}{ev\pi D^2}, \quad (1)$$

where I, v, and D represent the measured values of the streamer currents, streamer velocities, and optical diameters given in Figures 3, 4, and 5, respectively. With this approximation, we have assumed that (i) the radial component of the secondary electron drift flux is not significant, (ii) the streamer velocity is equal to the axial electron drift velocity, and (iii) the measured current is uniformly distributed over the area of the optical diameter. Under these assumptions, estimates of the electron number densities vs. applied voltage using Eq. (1) are given in Table I. These electron number density estimates range from approximately 5×10^{11} to 7×10^{11} cm^{-3} for increasing applied voltage with an uncertainty of 20%. The maximum electric field within the streamer head, E^*, can be related to the channel electron density behind the streamer head through the expression $n_e \approx (\varepsilon_o/e)\alpha^* E^*$,[10,18] where α^* is the ionization coefficient for helium evaluated for E^*. Using this expression with the values of number density given in Table I along with the functional dependence of α on the reduced electric field for pure helium,[32] we estimate that E^* is approximately 10 kV/cm–12 kV/cm at 520 Torr (60–70 Td) for the applied voltages range of 6–10 kV. This peak electric field estimate is in agreement with modeling results[10,11] and experiment[16] for helium gas guided streamers at atmospheric pressure. Note that modeled peak electric field for streamers in air at atmospheric pressure[11,17–22,24] are approximately an order of magnitude larger with corresponding electron densities on the order of 10^{14}–10^{15} cm^{-3}.[11,17–22,24]

We have also measured spatially (1 mm at the focal volume) and temporally (±2 ns) resolved optical emission from He 3^3D–2^3P transition at 587.6 nm, He 3^3S- 2^3P at 706.5 nm, N_2^+ 391 nm ($B^2\Sigma_u^+ \rightarrow X^2\Sigma_g^+$), and 337.1 nm emission from

N_2 $C^3\Pi_u$-$B^3\Pi_g$ using dual fiber coupled photomultipliers. The temporal variation of He 706.5 nm, N_2^+ 391 nm, and N_2 337.1 nm emissions has been measured with respect to the He 587.6 nm emission line. The normalized intensity plots for all those transitions are shown in Figure 7. In Figure 7, all traces have been corrected for cable signal propagation delays relative to the He 587.6 nm emission trace but not for the photo multiplier tube (PMT) transit time delays (47 ns). A correction for PMT transit time delays would result in a 47 ns shift of *all* waveforms earlier in time. For these measurements, the applied voltage was 9.4 kV, the streamer current probe front face was located 38 mm from the capillary tip, and the streamer velocity at the 16 mm location was 0.34 ± 0.05 mm/ns. There are two main features to note in Figure 7 that may help elucidate the N_2^+ 391 nm and N_2 337.1 nm emission intensity behavior for the helium gas guided streamer discharges with air or N_2-coflows. First, note that both the rise time and normalized peak emission intensities of the N_2^+ 391 nm and N_2 337.1 nm emission lines are time delayed by 5 ns and 11 ns, respectively, relative to the peak emission intensity of the He 587.6 nm line. Based on the streamer velocity measurement for the applied voltage condition, and assuming that the peak intensity of the He 587.6 nm line marks the streamer head, the N_2^+ 391 nm and N_2 337.1 nm peak emission intensities follow approximately 2 mm and 4 mm behind the streamer head, respectively. Furthermore, radial slice plots of the He 587.6 nm emission intensity obtained from ICCD imaging shown in Figures 8 and 9 indicate that the streamer head at the 16 mm location is always located well within the He gas core flow channel since the optical diameters are approximately one-third of the capillary tube (2 mm) inner diameter. These experimental observations indicate that *the head of the streamer is always located within the helium gas flow channel and co-flowing nitrogen plasma emissions are occurring behind the streamer head*. The N_2^+ ($B^2\Sigma_u^+$)

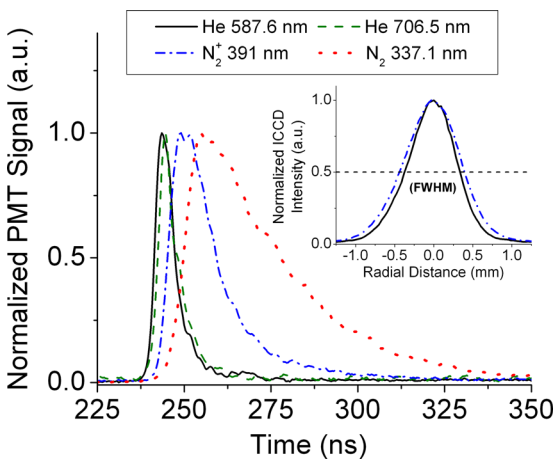

FIG. 7. Spectrally filtered normalized emission intensity traces of He 587.6 nm, He 706.5 nm, N_2^+ 391 nm, and N_2 337.1 nm transitions obtained using a dual fiber coupled-PMT optical system with the imaging volume transverse to the propagation axis and located 16 mm from the capillary tip. The inset shows normalized ICCD camera radial slice plots of the He 587.6 nm (solid line) and N_2^+ 391 nm (dash-dot line) emission intensities taken under similar conditions as the PMT data.

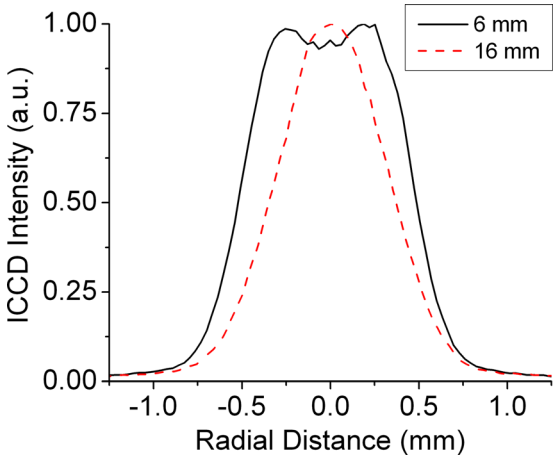

FIG. 8. Normalized radial slice plots taken from ICCD images of the He 587.6 nm emission intensity at gate delay times when the streamer head was located 6 mm (solid line) and 16 mm (dashed line) from the capillary tip. The total applied voltage was 6 kV and the pressure was 365 Torr.

population is probably produced by heavy particle energy transfer from helium metastable states at or near the co-flowing gas interface behind the streamer head because *the radial distribution of the reduced electric field is relatively*

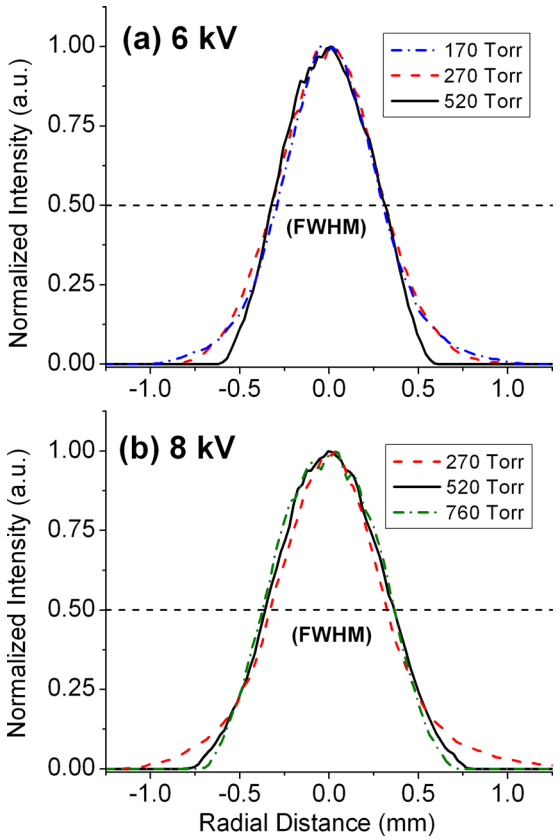

FIG. 9. Normalized radial slice plots taken from ICCD camera images of the He 587.6 nm emission intensity at a gate delay time when the streamer head was located 16 mm from the capillary tip. In both figures, the line shape FWHM represents the streamer optical diameter. In Figure 9(a), the total applied voltage was 6 kV for cell pressures 170 Torr (dashed dotted line), 270 Torr (dashed line), and 520 Torr (solid line). In Figure 9(b), the total applied voltage was 8 kV for cell pressures 270 Torr (dashed line), 520 Torr (solid line), and 760 Torr (dash–dotted line). During these measurements, the streamer current probe was located 23 mm from the capillary tip.

low near the diffusional mixing layer of the annular co-flow N_2 for the conditions shown in Figure 7. Thus, it is unlikely that both the core-flow helium and annular co-flow nitrogen gas will be simultaneously ionized at the streamer head for typical helium gas guided streamer discharges. We note that modeling results for a helium gas guided streamer having a peak axial reduced electric field of 70 Td *within a radially uniform* 1% air/helium mixture flow channel (see Figure 16 of Ref. 33) indicate that the peak electron impact excitation rate for N_2 $(C^3\Pi_u)_{v'=0}$ production also occurs behind the He ($n=3$) peak excitation rate. The second feature to note in Figure 7 are the N_2 337.1 nm and N_2^+ 391 nm e-fold decay times relative to the He 587.6 nm peak emission. With regards to N_2 337.1 nm emission, the model calculations shown in Figure 16 of Ref. 33 indicate that both the He ($n=3$) and N_2 $(C^3\Pi_u)$ state excitation rates decrease by 3 orders of magnitude within 0.05 mm behind their peak values. Assuming that both of these electron impact excitation rates turn off at their peaks in Figure 16 of Ref. 33, and using the effective radiative lifetime of 3 ns[34] for the $N_2(C^3\Pi_u)$ state quenched solely by N_2 $(X^1\Sigma^+_g)$, we estimate that the e-fold decay of the N_2 $(C^3\Pi_u)_{v'=0}$ population is 2.5 ns (~0.75 mm) behind the He ($n=3$) peak excitation rate. Under similar conditions of peak electric field, our data in Figure 7 shows that the e-fold decay time relative to the He 587.6 nm emission peak is 43 ns (15 mm). This implies that the prolonged decay of the N_2 337.1 emission intensity in Figure 7 is due to excitation through heavy particle kinetics (dissociative recombination of N_4^+). We note that the authors of Ref. 34 reach the same conclusion in their spectrally resolved experimental observations. Similarly, the N_2^+ $(B^2\Sigma_u^+)$ effective lifetime is approximately 0.2 ns in pure N_2.[34] In Figure 7, the e-fold decay time relative to the He 587.6 nm emission peak is 19 ns (6 mm), implying that the N_2^+ 391 nm emission within the channel is sustained by energy transfer from He 2 ^{3}S metastables.[35]

B. Variable pressure data

As mentioned in Sec. III A, the ICCD radial and axial emission profiles indicated that the influence of the Laplacian electric field extended to approximately 12 mm from the capillary tip. Figure 8 shows normalized radial intensity slice plots of He 587.6 nm emission for ICCD gate delay times when the streamer head maximum emission intensity was located 6 mm (solid line) and 16 mm (dashed line) from the capillary tip for a discharge condition of 6 kV applied voltage at 365 Torr. Both normalized radial intensity slice plots in Figure 8 were obtained from background subtracted ICCD images using ImageJ and are the result of a 10 pixel binning average in the axial direction at the maximum emission intensity. At 6 mm, the intensity profile exhibits two peak emission intensities at approximately ±0.25 mm away from the propagation axial centerline. This emission profile indicates that the streamer has a ring-like morphology that is formed, initially, along the inside of the 2 mm diameter dielectric capillary tube wall by the Laplacian electric field generated at the ring anode.[8,10,14,29] As the streamer propagates out of the capillary tip to 6 mm distance, shown in Figure 8, it is guided by the ring shaped Laplacian electric field in the helium jet which is surrounded by the N_2 co-flow gas[10,14] and driven by both the superimposed Laplacian and Poisson electric fields. From radial and axial emission intensity slice plots obtained from ICCD imaging, we observed that the two off-axis emission intensity peaks converge into a single peak on axis occurring approximately 10 mm from the capillary tip. However, axial intensity slice plots of the ICCD emission at 9 kV and 10 kV applied voltages indicated that the Laplacian electric field extended up to approximately 12 mm. At 16 mm, the Laplacian electric field is negligible for all applied voltage and pressure conditions studied, and the normalized Gaussian-like emission intensity profile, shown in Figure 8, represents emission intensity produced from the self-consistent Poisson electric field at the streamer head. All pressure scaling properties of the streamer data presented in this section have been studied under the conditions of Poisson electric field dominated propagation dynamics located 16 mm from the capillary tip.

Figure 9 shows pressure dependent normalized He 587.6 nm ICCD emission intensity radial slice plots obtained at (a) 6 kV for cell pressures 170 Torr, 270 Torr, and 520 Torr, and (b) 8 kV for cell pressures 270 Torr, 520 Torr, and 760 Torr. Each radial intensity slice plot was obtained by binning 10 pixels in the axial direction at the maximum emission intensity of the streamer. The optical diameters in Figures 9(a) and 9(b) have been denoted by the FWHM. Note that the optical diameters at 520 Torr in both Figures 9(a) and 9(b) correspond to those plotted in Figures 5 and 6 at 6 kV and 8 kV. The optical diameter measurements as a function of pressure for 6 kV and 8 kV are given in Table II. At 6 kV, the optical diameters increase slightly (within the 13% measurement uncertainty) and can be considered nearly constant. At 8 kV, the increase in optical diameters is approximately 14% larger compared to 6 kV, but the variation is still near the imaging resolution limit. These results indicate that the optical diameters obtained from the helium guided streamer are essentially invariant within the pressure range studied at 6 kV and 8 kV applied voltages. Furthermore, the streamer velocities are also invariant to optical diameter, similar to that of Figure 6, when displayed on a velocity-diameter plot (not shown). The invariance of the optical diameter with pressure for the helium guided streamer again exhibits a strong departure from the predicted inverse gas density

TABLE II. Pressure dependent measurements (see Figure 9) of streamer optical diameters and estimates of peak electron number densities for 6 kV and 8 kV total applied voltages. The uncertainty of the diameter measurements are ±13% while that of the number density estimates are ±20%.

Applied voltage	6 kV		8 kV	
p (Torr)	D (mm)	n_e ($\times 10^{11}$ cm^{-3})	D (mm)	n_e ($\times 10^{11}$ cm^{-3})
170	0.58	8.3	…	…
210	0.60	7.0	…	…
270	0.63	6.7	0.67	8.2
365	0.63	5.7	0.70	7.0
520	0.63	5.5	0.74	6.0
760	…	…	0.75	5.5

dependence based upon similarity scaling and confirmed by measurements[24,25] and modeling[17] in both N_2 and air. Furthermore, the invariance of optical diameter with streamer velocity is also in strong contrast to measurements[17,24,25] and 2-D model calculations[17] for streamer discharges in both N_2 and air.

The streamer velocity and peak streamer current pressure scaling are shown in Figure 10 as a function of inverse pressure for both 6 kV and 8 kV applied voltages (squares and circles, respectively). Note that the data shown in Figure 10 correspond to the same data set presented in Figure 9 with the addition of a set taken at 6 kV, 210 Torr. The "best fit" polynomial (see Sec. III A) that describes the scaling is linear with inverse pressure for both streamer velocities (solid lines) and peak currents (dashed lines) for both applied voltages. Thus, both streamer velocity and peak streamer current vary inversely proportional to pressure at 6 kV and 8 kV. At 6 kV and 8 kV the fitted slopes for the velocity are [132.248 ± 17.129 Torr·mm/ns] and [201.692 ± 19.656 Torr·mm/ns], respectively. The fitted peak current slopes at 6 kV and 8 kV are [5015.585 ± 717.576 Torr·mA] and [10240.298 ± 2071.687 Torr·mA], respectively. This inverse pressure scaling is in agreement with both measurements and modeling performed for streamers in air.[17]

IV. ANALYSIS AND DISCUSSION

In this work, the invariance of the optical diameter scaling with applied voltage, streamer velocity, and gas pressure exhibits the most striking difference between self-sustained low dielectric strength helium guided streamer with nitrogen co-flow and that of streamer propagation in homogeneous air or nitrogen. For the 2 mm I.D. CDBD operating with 2 SLM helium flow at 520 Torr, peak streamer current measurements with applied voltage as shown in Figure 3 imply that diffusional mixing of the co-flowing N_2 gas into the helium core flow is negligible for self-sustained streamer propagation up to approximately 33 mm from the capillary tip. For each repetitively pulse discharge, the normalized radial slice plots shown in Figure 9 indicate that the Poisson electric field driven positive streamer propagates well within the pure helium core flow as indicated by the extent of the optical diameter relative to the 2 mm capillary tube inner diameter.

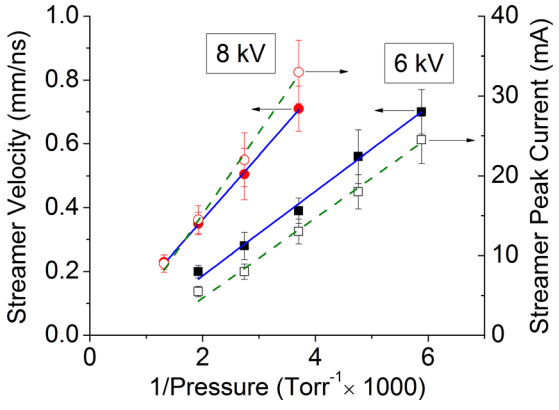

FIG. 10. Streamer velocities (closed symbols) and corresponding peak currents (open symbols) measured as a function of inverse pressure for total applied voltages of 6 kV (squares) and 8 kV (circles). The streamer velocities were measured 16 mm from the capillary tip with the streamer current probe front face located 23 mm from the capillary tip. The solid and dashed lines are linear best fits (see text) to the measured speed and peak current data points, respectively.

Certainly, the higher dielectric breakdown strength of the surrounding N_2 co-flow confines the streamer propagation to within the helium gas channel as its morphology transitions from ring-shaped to a highly localized Gaussian-like radial profile.[10,12] We have experimentally verified this by substituting N_2 co-flowing gas with helium at atmospheric pressure, with the result that the helium plasma extending beyond the glass capillary is no longer a gas guided streamer. The invariance of the optical diameter versus applied voltage, streamer speed, and gas pressure within the pure helium core flow is a consequence of this disparity in the gas breakdown strengths but more importantly, it is due to relatively higher remnant ionization within the pure helium core compared to that of the helium-nitrogen mixing layer (discussed below). If the timescale of electron-ion recombination within the pure helium core is significantly longer than that within the mixing layer during the pulse discharge period, then successive streamers will propagate through remnant pre-ionization that is preferentially higher within the pure helium core relative to that within the mixing layer. This could result in the highly localized streamer propagation within the pure helium core as shown in our experimental results.

We have constructed a 0-D onset condition model by which we qualitatively demonstrate the evolution of streamer localization due to remnant ionization at the end of the first discharge pulse. With this model, electron losses are compared at the end of our experimental 200 μs pulse repetition period due to electron-ion recombination within the pure helium core to those within the N_2-He mixing region (up to 1% N_2 admixture) for the experimental condition of 520 Torr. In Sec. III A, the estimated electron number density behind the streamer head for the applied voltage range 6–10 kV is approximately 6×10^{11} cm^{-3} (see Table I) corresponding to a maximum electric field within the streamer head of about 11 kV/cm (65 Td). Table III shows the elementary reaction set and rate coefficients used in the model[32,36–39] for the dominant ionic species that participate in (i) direct electron impact ionization, (ii) ion conversion, and (iii) electron-ion recombination. We used Bolsig+[32] to calculate the direct ionization rate coefficients (R1)–(R3) for 65 Td, 520 Torr conditions. The ionization rate coefficient in Table I for helium (R3) is an average of the ionization coefficients computed for pure helium and a 1% N_2-He admixture, while those for N_2^+(X) (R1) and N_2^+(B) (R2) were computed for a 1% N_2-He admixture.

Before discussing the numerical calculations, we first considered analytical estimates of the remnant ionization (also elucidating the dominant recombination mechanism) at the end of the 200 μs pulse repetition period for the limiting cases of (i) pure helium and (ii) 1% N_2-He admixture with background gas conditions of 520 Torr and 300 K. In the case of pure helium, the net loss rate of electrons due to recombination is (see Table III),

TABLE III. Elementary reactions and rate coefficients used in the zero-dimensional model.

Reaction no.	Reaction	Rate coefficient	Reference
Direct electron impact ionization, 65 Td and 520 Torr			
R1	$e + N_2 \rightarrow N_2^+(X) + 2e$	1.76×10^{-9} cm^3/s (1% N_2/He)	32
R2	$e + N_2 \rightarrow N_2^+(B) + 2e$	1.04×10^{-10} cm^3/s (1% N_2/He)	32
R3	$e + He \rightarrow He^+ + 2e$	8.58×10^{-11} cm^3/s (avg., see text)	32
Ion conversion			
R4	$N_2^+ + 2N_2 \rightarrow N_4^+ + N_2$	5×10^{-29} cm^6/s	36
R5	$He^+ + 2He \rightarrow He_2^+ + He$	6.5×10^{-32} cm^6/s	37
R6	$He_2^+ + N_2 \rightarrow N_2^+ + He_2$	1.4×10^{-9} cm^3/s	39
Electron-ion recombination			
R7	$e + N_2^+ \rightarrow N + N$	$2.8 \times 10^{-7}(300\,\mathrm{K}/T_e)^{0.5}$ cm^3/s	36
R8	$e + N_2^+ \rightarrow N + N(^2D)$	$2 \times 10^{-7}\,(300\,\mathrm{K}/T_e)^{0.5}$ cm^3/s	36
R9	$e + He_2^+ \rightarrow He + He$	3.3×10^{-10} cm^3/s at 300 K	38
R10	$e + N_4^+ \rightarrow N_2 + N_2$	$2 \times 10^{-6}\,(300\,\mathrm{K}/T_e)^{0.5}$ cm^3/s	37 and 43
R11	$2e + He_2^+ \rightarrow He^m + He + e$	$4 \times 10^{-20}\,(T_g/T_e)^4$ cm^6/s	37
R12	$e + He + He_2^+ \rightarrow He^m + 2He$	$5 \times 10^{-27}\,(T_g/T_e)$ cm^6/s	37
R13	$2e + He^+ \rightarrow He + e$	$8 \times 10^{-20}\,(T_g/T_e)^4$ cm^6/s	37
R14	$2e + N_2^+ \rightarrow e + N_2$	$1 \times 10^{-19}\,(300\,\mathrm{K}/T_e)^{4.5}$ cm^6/s	36
R15	$e + N_2^+ + N_2 \rightarrow N_2 + N_2$	$6 \times 10^{-27}\,(300\,\mathrm{K}/T_e)^{1.5}$ cm^6/s	36

$$\frac{dn_e}{dt} = -\beta_9 n_{He_2^+} - \beta_{11} n_{He_2^+} - \beta_{12} n_{He} n_{He_2^+} n_e - \beta_{13} n_{He^+} n_e^2, \tag{2}$$

where β_x are the recombination rate coefficients (R9), (R11)–(R13) in Table III and n_x represent the ion, electron, and neutral gas number densities. Note that the electron density (6×10^{11} cm^{-3}) remains constant during ion conversion so it then becomes the initial condition for the recombination process. In addition, we have assumed that the electron temperature during recombination is equal to the neutral gas temperature, 300 K. The timescale for ion conversion is typically much faster than that of electron-ion recombination.[40] At 520 Torr, $He^+ \rightarrow He_2^+$ (R5) ion conversion timescale is approximately 56 ns while that of the atomic ion recombination term (R13) is approximately 50 μs for an initial electron number density $n_{e,0} = 6 \times 10^{11}$ cm^{-3}. Thus, all He^+ ions convert to He_2^+ prior to recombination so that the last rate term in Eq. (2) is negligible. Charge conservation requires that the He_2^+ density equals that of the electrons during recombination, allowing us to estimate the magnitudes of the three remaining terms in Eq. (2). The rate of three-body dissociative recombination (R12) dominates those of (R9) and (R11) by at least an order of magnitude, so that Eq. (2) has the approximate solution[40]

$$n_e(t) = \frac{n_{e,0}}{1 + n_{e,0}\beta_{12} n_{He} t}, \tag{3}$$

where $n_e(t=0) = n_{e,0} = 6 \times 10^{11}$ cm^{-3} and n_{He} is the neutral background helium density. Note that the initial time can be defined as $t = 0$ ns with good approximation because of the comparatively long electron-ion recombination timescale. Evaluating Eq. (3) just before the next excitation pulse at 200 μs, we find that $n_e \approx 5 \times 10^{10}$ cm^{-3} within the pure helium core.

The net electron recombination rate equation for a 1% N_2-He mixture at 520 Torr, 300 K (reactions R7-R15) is

$$\begin{aligned}\frac{dn_e}{dt} = &-\beta_{7,8} n_{N_2^+} n_e - \beta_9 n_{He_2^+} n_e - \beta_{10} n_{N_4^+} n_e \\ &- \beta_{11} n_{He_2^+} n_e^2 - \beta_{12} n_{He} n_{He_2^+} n_e - \beta_{13} n_{He^+} n_e^2 \\ &- \beta_{14} n_{N_2^+} n_e^2 - \beta_{15} n_{N_2} n_{N_2^+} n_e,\end{aligned} \tag{4}$$

where $\beta_{7,8} = \beta_7 + \beta_8$. Equation (4) can be greatly simplified because, again, the ion conversion and electron-ion recombination occur nearly in series on very different timescales. The ion conversion pathway in this case is $He^+ \rightarrow He_2^+ \rightarrow N_2^+ \rightarrow N_4^+$. For these conditions, the conversion of $He_2^+ \rightarrow N_2^+$ is much faster (4 ns) than that of $N_2^+ \rightarrow N_4^+$ (1 μs). By the end of the ion conversion process, N_4^+ becomes the dominant ion and is equal to the electron density during recombination. We note that total ion conversion to N_4^+ occurs on a similar timescale as that of the N_4^+ dissociative recombination reaction (R10), but the numerical solution discussed below indicates that this is a good approximation. The net electron number density rate equation has the solution

$$n_e(t) = \frac{n_{e,0}}{1 + n_{e,0}\beta_{10} t}, \tag{5}$$

where $n_e(t=0) = n_{e,0} = 6 \times 10^{11}$ cm^{-3}. Evaluating Eq. (5) at the end of the pulse period, we find $n_e \approx 2.5 \times 10^9$ cm^{-3} within the 1% N_2-He mixing layer. These analytic estimates for electron-ion recombination at 520 Torr indicate that the *remnant ionization within the pure helium core at the end of the 200 μs pulse period is an order of magnitude greater than that within the 1% N_2-He mixing layer*.

Figures 11(a)–11(c) show the results of solving the set of time dependent net rate equations for electron, He^+, He_2^+, N_2^+, and N_4^+ densities at 520 Torr, 300 K neutral gas temperature, and pre-ionization density of 10^8 cm^{-3} for (a) pure helium, (b) 0.01% N_2-He, and (c) 1% N_2-He admixtures using the 4th Order Runge-Kutta method.[41] In this 0-D model, we have assumed that the electron and gas temperatures are equal

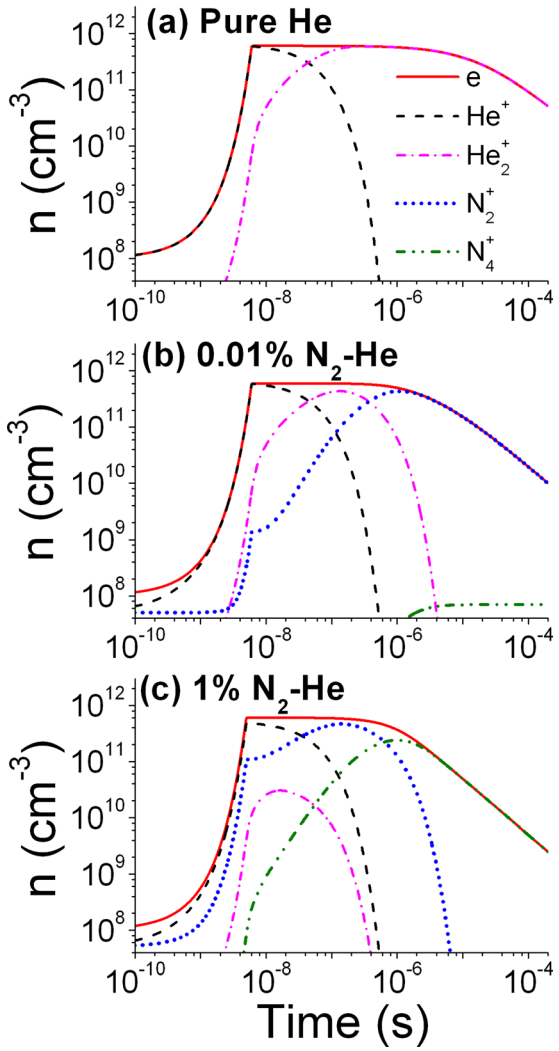

FIG. 11. Zero-dimensional modeling results of electron (solid line), He^+ (dash), He_2^+ (dash-dot), N_2^+ (dotted), and N_4^+ (dash-dot-dot) number densities vs. time for the cases of (a) pure helium, (b) 0.01% N_2-He admixture, and (c) 1% N_2-He admixture.

during electron-ion recombination. We have chosen the value of 0.01% N_2-He in Figure 11(b) because it approximately demarcates the admixture for which the nitrogen ion species begin to play a significant role in ion conversion and recombination and therefore, becomes an upper bound for which the core flow can be considered as "pure" helium. In each case shown in Figures 11(a)–11(c), we have modeled the passing of the self-propagating electric field at 65 Td as a square pulse during which we have solved the rate equations (R1)–(R6) until the electron number density reached $6 \times 10^{11}\,cm^{-3}$. The time to reach this electron density (solid line) was approximately 5 ns and was practically independent of nitrogen admixture (note that this computed rise time varied between approximately 2 and 10 ns for pre-ionization densities between 10^{10} and $10^{4}\,cm^{-3}$, respectively). This time is much shorter than the measured streamer current rise time of 70 ns shown in Figure 2 (Sec. III A). Since the streamer current rise time may be impacted due to electron drift through the streamer channel and Pearson probe circuit, we have used the results of the He (3^3D-2^3P) 587.6 nm emission intensity rise time acquired using the side-view PMT shown in Figure 7 as well as ICCD camera axial slice plots (not shown) taken with a 5 ns gate for comparison. The He 587.6 nm rise time using the PMT in Figure 7 was about 3 ns while that using the ICCD camera was 5 ns. Hence, Figures 11(a)–11(c) show that the calculated time to reach an electron number density of $6 \times 10^{11}\,cm^{-3}$, which was estimated using experimentally measured quantities expressed by Eq. (1), are in qualitative agreement with that of two independent He (3^3D-2^3P) 587.6 nm emission intensity rise time measurements.

Figure 11(a) shows the results for the case of pure helium in which all of the He^+ population (dashed line) converted to He_2^+ (dash-dotted line) after 1 μs, and the remnant ionization is $5 \times 10^{10}\,cm^{-3}$ after 2×10^{-4} s (200 μs), in agreement with the approximation using Eq. (3). For pure helium, only the three-body electron-ion recombination reaction (R12) had any effect on the electron decay rate, which is again consistent with the approximation for obtaining Eq. (3). For the nitrogen admixtures shown in Figures 11(b) and 11(c), we did not use reaction (R12) because helium metastables are rapidly quenched through Penning ionization with subsequent nitrogen ion conversion and dissociative recombination. Figure 11(b) shows the results for 0.01% N_2-He admixture. In this case, both He^+ and He_2^+ are converted into N_2^+ (dotted line), which has a maximum of $4 \times 10^{11}\,cm^{-3}$ at about 1 μs. Note that the N_4^+ (dash-dot-dotted line) population, produced via ion conversion reaction (R4), is less than $10^{8}\,cm^{-3}$ and that the dissociative recombination reaction R(10) has no effect on the electron decay rate. The electron decay rate is due solely to N_2^+ dissociative recombination reactions (R7) and (R8) and the remnant ionization at 200 μs is $1 \times 10^{10}\,cm^{-3}$ (five times smaller than that of pure helium). Figure 11(c) shows the results for the 1% N_2-He admixture. In this case, the concentration of neutral nitrogen is sufficient that the sequential ion conversion pathway $He_2^+ \rightarrow N_2^+$ leads to N_4^+ (R4) becoming the dominant ion ($2 \times 10^{11}\,cm^{-3}$) within 1 μs. The dissociative recombination of N_2^+ (R7 and R8) was found to affect the onset of electron decay at about 0.1 μs, but, as the dominant ion species concentration switched from N_2^+ to N_4^+ at approximately 1 μs, dissociative recombination (R10) became the dominant electron loss mechanism. The remnant ionization in Figure 11(c) at 200 μs is $2.5 \times 10^{9}\,cm^{-3}$ and is the same result obtained using the approximate Eq. (5).

V. CONCLUSION

The 0-D electron-ion recombination model shows that within the gas mixing layer where the nitrogen concentration is 1%, the remnant ionization after 200 μs is more than an order of magnitude smaller than that within the pure helium channel, assuming that the reduced electric field at the streamer head is 65 Td and the electron number density behind the streamer is on the order of $6 \times 10^{11}\,cm^{-3}$. If the self-propagating electric field at the streamer head has a similar Gaussian-like profile as shown by the He (3^3D-2^3P) 587.6 nm emission measurements in Figure 9, then the remnant ionization in the mixing layer will be lower than these estimates compared to the pure helium channel. This suggests that under our experimental conditions of 5 kHz pulse

repetition rate, 16 mm from the capillary tip, it is the electron-ion recombination rates, rather than the direct ionization rates within the 1% mixing layer,[11,12] that maintain a dominant conductive channel within the pure helium gas core which guides streamer propagation and prohibits streamer branching with increase in applied voltage. In other words, for typical CDBD reduced electric fields, the lower dielectric breakdown strength of the helium gas channel compared to the surrounding nitrogen annular co-flow and the electron loss rates (rather than direct ionization production rates) become the proper boundary conditions that lead to the observed invariance of the optical diameter with applied voltage, streamer velocity, and gas pressure.

Without diffusional mixing of air or nitrogen, guided helium streamer model simulations[10] indicate that the initial externally applied Laplacian electric field is responsible for the formation and guiding of the ring-shaped streamer into the helium core flow outside the dielectric tube, rather than direct electron impact ionization at the 1% helium-air mixing layer.[11,12] The simulations[10] also show that the high off-axis ionization region converges towards the axis faster in time as the initial uniform pre-ionization density decreases from $10^8\,cm^{-3}$ to $10^4\,cm^{-3}$, which is consistent with a larger on-axis electric field.[10] With the effect of diffusional mixing, the confinement of the ring-shaped ionization region may also be a consequence of electron-ion recombination, rather than direct electron impact ionization, in addition to the difference in breakdown strengths of helium versus nitrogen. The Laplacian electric field is then responsible for guiding the streamer into the helium core flow upon exiting the dielectric tube rather than the 1% helium-nitrogen mixing layer.

Finally, the temporal variation of both rise times and decay times of emission intensity plots in Figure 7 show that only helium emission lines are excited by direct electron impact. Both N_2 C-B and N_2^+ B-X emission lines are produced by heavy particle kinetics. The N_2^+ B-X emission line is most likely produced by the energy transfer from $He(2\,^3S) + N_2 \rightarrow N_2^+ B + He$ with measured rate constant $1 \times 10^{-9}\ cm^3/s$.[42] The N_2 C state excitation is produced by $N_4^+ + e \rightarrow N_2\ (C^3\Pi_u) + N_2$ with measured dissociative recombination rate constant of $2.6 \times 10^{-6}\ cm^3/s$ at 300 K.[43] The N_2 C $\rightarrow$ B 337.1 nm emission marks the dissociative recombination reaction of N_4^+ ions in streamer channel behind the streamer head.

ACKNOWLEDGMENTS

We wish to thank Dr. Alan Garscadden for discussion and his comments on the manuscript. Funding for this research was provided by the Air Force Office of Scientific Research (Dr. Jason Marshall, Program Manager).

[1]M. Teschke, J. Kedzierski, E. Finantu-Dinu, D. Korzec, and J. Engemann, IEEE Trans. Plasma Sci. **33**, 310 (2005).
[2]M. Laroussi and X. Lu, Appl. Phys. Lett. **87**, 113902 (2005).
[3]J. Walsh, J. Shi, and M. Kong, Appl. Phys. Lett. **88**, 171501 (2006).
[4]J. L. Walsh, F. Iza, N. B. Janson, V. J. Law, and M. G. Kong, J. Phys. D: Appl. Phys. **43**, 075201 (2010).
[5]K. Gazeli, C. Noël, F. Clément, C. Daugé, P. Svarnas, and T. Belmonte, Plasma Sour. Sci. Technol. **22**, 025020 (2013).
[6]B. Sands, B. Ganguly, and K. Tachibana, Appl. Phys. Lett. **92**, 151503 (2008).
[7]K. Urabe, Y. Ito, K. Tachibana, and B. Ganguly, Appl. Phys. Express **1**, 066004 (2008).
[8]Q. Th. Algwaril and D. O'Connell, Appl. Phys. Lett. **99**, 121501 (2011).
[9]E. Robert, V. Sarron, D. Ri'es, S. Dozias, M. Vandamme, and J.-M. Pouvesle, Plasma Sour. Sci. Technol. **21**, 034017 (2012).
[10]J. P. Boeuf, L. L. Yang, and L. C. Pitchford, J. Phys. D: Appl. Phys. **46**, 015201 (2013).
[11]G. V. Naidis, J. Phys. D: Appl. Phys. **44**, 215203 (2011).
[12]D. Breden, K. Miki, and L. L. Raja, Plasma Sour. Sci. Technol. **21**, 034011 (2012).
[13]Q. Li, Y. Pu, M. A. Lieberman, and D. J. Economou, Phys. Rev. E **83**, 046405 (2011).
[14]J. Jánský and A. Bourdon, Appl. Phys. Lett. **99**, 161504 (2011).
[15]Y. Sakiyama, D. Graves, J. Jarrige, and M. Laroussi, Appl. Phys. Lett. **96**, 041501 (2010).
[16]A. Sobota, O. Guaitellaand, and E. Garcia-Caurel, J. Phys. D: Appl. Phys. **46**, 372001 (2013).
[17]S. Pancheshnyi, M. Nudnova, and A. Starikovskii, Phys. Rev. E **71**, 016407 (2005).
[18]N. Yu. Babaeva and G. V. Naidis, J. Phys. D: Appl. Phys. **29**, 2423–2431 (1996).
[19]S. V. Pancheshnyi and A. Starikovskii, J. Phys. D: Appl. Phys. **36**, 2683–2691 (2003).
[20]G. Naidis, Phys. Rev. E **79**, 057401 (2009).
[21]A. Luque and U. Ebert, Phys. Rev. E **84**, 046411 (2011).
[22]A. Komuro, R. Ono, and T. Oda, Plasma Sour. Sci. Technol. **22**, 045002 (2013).
[23]T. T. J. Clevis, S. Nijdam, and U. Ebert, J. Phys. D: Appl. Phys. **46**, 045202 (2013).
[24]U. Ebert, S. Nijdam, C. Li, A. Luque, T. Briels, and E. van Velduizen, J. Geophys. Res. **115**, A00E43, doi:10.1029/2009JA014867 (2010) and references therein.
[25]S. Nijdam, F. M. J. H. van de Wetering, R. Blanc, E. M. van Veldhuizen, and U. Ebert, J. Phys. D: Appl. Phys. **43**, 145204 (2010).
[26]T. M. P. Briels, J. Kos, G. J. J. Winands, E. M. van Veldhuizen, and U. Ebert, J. Phys. D: Appl. Phys. **41**, 234004 (2008).
[27]See http://physics.nist.gov/PhysRefData/ASD for National Institute of Standards and Technology Physics Laboratory Physical Reference Data Atomic and Spectral Database.
[28]See www.OriginLab.com for OriginPro 8.1, OriginLab Corp., Northampton, MA, 2010.
[29]R. Leiweke, B. Sands, and B. Ganguly, IEEE Trans. Plasma Sci. **39**(11), 2304 (2011).
[30]W. S. Rasband, see http://imagej.nih.gov for ImageJ 1.47, U.S. National Institutes of Health, Bethesda, Maryland, USA.
[31]D. G. Kleinbaum, L. L. Kupper, K. E. Muller, and A. Nizam, *Applied Regression Analysis and Other Multivariable Methods*, 3rd ed. (Duxbury Press, New York, 1998), pp. 281–292, Chap. 13.
[32]G. J. M. Hagelaar and L. C. Pitchford, Plasma Sour. Sci. Technol. **14**, 722 (2005).
[33]G. V. Naidis and J. L. Walsh, J. Phys. D: Appl. Phys. **46**, 095203 (2013).
[34]K. V. Kozlov, R. Brandenburg, H.-E. Wagner, A. M. Morozov, and P. Michel, Phys. D: Appl. Phys. **38**, 518–529 (2005).
[35]K. Urabe, T. Morita, K. Tachibana, and B. N. Ganguly, J. Phys. D: Appl. Phys. **43**, 095201 (2010).
[36]I. A. Kossyi, A. Yu. Kostinsky, A. A. Matveyev, and V. P. Silakov, Plasma Sour. Sci. Technol. **1**, 207 (1992).
[37]R. Deloche, P. Monchicourt, M. Cheret, and R. Lambert, Phys. Rev. A **13**, 1140–1176 (1976).
[38]H. B. Pedersen, H. Buhr, S. Altevogt, V. Andrianarijaona, H. Kreckel, L. Lammich, N. de Ruette, E. M. Staicu-Casagrande, D. Schwalm, D. Strasser, X. Urbain, D. Zajfman, and A. Wolf, Phys. Rev. A **72**, 012712 (2005).
[39]Yu. B. Golubovskii, V. A. Maiorov, J. Behnke, and J. F. Behnke, J. Phys. D: Appl. Phys. **36**, 39–49 (2003).
[40]Y. P. Raizer, *Gas Discharge Physics* (Springer-Verlag, New York, 1997), p. 60, Sec. 4.3.1.
[41]C. R. Wylie and L. C. Barrett, *Advanced Engineering Mathematics*, 5th ed. (McGraw-Hill Book Co., New York, 1982), pp. 271–273.
[42]J. M. Pouvesle, A. Bouchoule, and J. Stevefelt, J. Chem. Phys. **77**, 817 (1982).
[43]Y. S. Cao and R. Johnsen, J. Chem. Phys. **95**, 7356 (1991).